EXAFS Study of Micellar Aggregates of Bile Acid Rubidium Salts

P. D'Angelo, A. Di Nola, E. Giglio, M. Mangoni, and N. V. Pavel*

Dipartimento di Chimica, Università degli Studi di Roma "La Sapienza", P.le Aldo Moro 5, 00185 Rome, Italy

Received: July 28, 1994; In Final Form: December 2, 1994[⊗]

Extended X-ray absorption fine structure (EXAFS) spectroscopy has been employed to characterize the local environment of the Rb^+ ions in micellar aggregates of bile acid rubidium salts. In a previous study at the Rb K-edge it was found that the Rb^+ ions of the rubidium deoxycholate (RbDC) micellar aggregates have the same or a very similar coordination as that of the helical structure in the crystal, which is remarkably different from the coordination of the aqueous solvated Rb^+ ions. In the present paper we report the EXAFS data analysis of crystals and aqueous micellar solutions of rubidium taurodeoxycholate (RbTDC), rubidium glycodeoxycholate (RbGDC), and rubidium glycocholate (RbGC). Crystals and micellar solution spectra are compared with a theoretical signal calculated for a coordination model of a Rb^+ ion surrounded by water molecules by employing the Rb−O radial distribution function obtained from molecular dynamics simulations and refined by using the EXAFS spectrum of a RbOH aqueous solution. This strategy has been successfully checked by analyzing the EXAFS spectrum of a RbDC aqueous micellar solution. The crystal spectra of RbTDC and RbGC agree with the Rb^+ coordination observed in their known crystal structures, whereas that of RbGDC indicate that the Rb^+ coordination is liquidlike in the corresponding crystal of unknown structure. The spectra of the aqueous solutions, containing micellar aggregates of small size, show that the Rb^+ ions are exposed to or dipped into the solvent and allow some structural models for the micellar aggregates to be discarded.

Introduction

Bile salts and their conjugated derivatives can be considered one of the most important class of natural detergents. In aqueous solutions they give rise to micellar aggregates and interact with several biological compounds such as cholesterol, bilirubin-IXα, phospholipids, glycerides and fatty acids. They are present in the bile, where they are involved in many regulatory mechanisms, and they play a pivotal role in the emulsifying process of the dietary lipids in the small intestine.[1] Due to their solubilization properties, many efforts have been made to determine the micellar structure of the bile salts. However, the experimental data available for these systems in solution do not provide enough information to acquire definite models of the micellar aggregates.

Surfactants with a very similar structural unit in both the liquid and solid phase can be studied by resorting to structural models obtained from the crystalline state. The structural unit of well-defined geometry observed in a crystal can be checked as a possible model of the micellar aggregate. This strategy was previously used in the case of sodium and rubidium deoxycholate[2] (NaDC and RbDC, respectively). The crystal structures of NaDC and RbDC are characterized by similar helical units[2−4] which were used to describe the behavior of the micellar solutions. The helical structure of the micellar aggregates was verified by means of several techniques such as nuclear magnetic resonance,[2,5−7] circular dichroism[7−9] (CD), electron spin resonance,[10] small-angle X-ray scattering[10] (SAXS), extended X-ray absorption fine structure (EXAFS) spectroscopy,[11−13] and electromotive force measurements of galvanic cells containing electrodes reversible to sodium, hydrogen, and deoxycholate ions.[14]

In particular, the EXAFS technique is sensitive to the local coordination of an excited atom or ion. It was employed to compare the Rb^+ coordination in the RbDC crystal with that of the fiber and of the micellar aggregates.[11] Since the Rb^+ ions are located inside the helix of the RbDC crystal, if the micellar aggregates have the same or a similar helical structure, the Rb^+ ions will maintain the same or a similar coordination as in the crystal. Moreover, the peculiar Rb^+−O radial distribution function of the crystal is certainly different from that of Rb^+ ions dissolved in water. From an EXAFS study at the Rb K-edge, it was found that the Rb^+ ions of the RbDC micellar aggregates have the same or a very similar coordination as that of the crystal, which is remarkably different from the coordination of the aqueous solvated Rb^+ ions.[11]

The same strategy can be applied to other bile acid salts. Lately, several crystal structures of bile acid salts were solved, namely those of sodium taurodeoxycholate[15] (NaTDC), rubidium taurodeoxycholate[16] (RbTDC), sodium glycodeoxycholate[9] (NaGDC), sodium glycocholate[17] (NaGC), and the triclinic[18] and monoclinic[19] phases of sodium taurocholate (NaTC). Furthermore, the crystal structure of rubidium glycocholate (RbGC) and that of a monoclinic phase of NaTDC were solved but not yet published.[20] The most recurrent structures observed in crystals were helices with a 6-fold,[2,9] pseudo-6-fold,[4] 3-fold,[15] or 2-fold screw axis[16,17,19] and a structural unit with a 2-fold rotation axis.[19] The triclinic phase of NaTC and the monoclinic one of RbGC are formed by bilayers as in the case of sodium cholate[21] and RbDC[22] crystals grown from organic solvents. Only structural units characterized by 2-fold screw or rotation axes or by bilayers were observed in the crystal structures of the trihydroxy salts.

A preferential interaction of the NaDC, RbDC, NaGDC, and NaTDC micellar aggregates with the left-handed enantiomeric conformer of bilirubin-IXα (BR) was pointed out by CD measurements.[7,9] Subsequently, a study of the enantioselective complexation of BR in aqueous micellar solutions of NaTDC, RbTDC,[16] NaTC, and RbTC[19] showed a strong similarity to

[⊗] Abstract published in *Advance ACS Abstracts,* March 15, 1995.

0022-3654/95/2099-5471$09.00/0

the CD spectra of the dihydroxy salts on one hand and of the trihydroxy salts on the other. Moreover, X-ray diffraction studies showed that NaTDC, RbTDC, NaGDC and rubidium glycodeoxycholate (RbGDC) give nearly equal helical fibers.[16,23] On the other hand, the trihydroxy salts do not form helical fibers, have greater critical micellar concentrations and lower aggregation numbers than the dihydroxy salts under the same conditions, and are characterized by a weak ability to associate. Thus, on the basis of the CD and X-ray results two different types of structural units can be proposed at least for the micellar aggregates of the dihydroxy and trihydroxy salts.

In the present paper, we report the EXAFS data analysis of the RbTDC, RbGDC, and RbGC crystals (cRbTDC, cRbGDC, and cRbGC, respectively) and aqueous solutions (sRbTDC, sRbGDC, and sRbGC, respectively) at the Rb K-edge. The EXAFS data analysis is usually performed by describing the coordination of the photoabsorber atom with a set of Gaussian shells, both in the solid and in the liquid state. A more correct description of disordered systems in the real space may be performed in terms of radial distribution function $g(r)$. Recently, a new EXAFS data analysis method has been presented[24] which allows the use of pair correlation functions as relevant models in the calculation of the EXAFS signal. This method has been successfully applied to the case of aqueous solutions of rubidium bromide, bromoethane, and 2-bromopropane. The EXAFS spectra have been analyzed at the Br K-edge by employing the Br−O radial distribution function obtained from molecular dynamics (MD) simulations.

In the present work the Rb−O pair distribution function obtained from MD simulations is used to calculate the water contribution to the EXAFS spectrum of a RbOH aqueous solution. This approach provides a satisfactory model of the solvent surrounding the Rb^+ ion. The comparison of the signal obtained from the fitted MD $g_{Rb,O}(r)$ with the micellar solution spectra of RbDC, RbTDC, RbGDC, and RbGC allows the micellar systems, in which the Rb^+ ions are exposed to the solvent or do not present a peculiar coordination, to be identified. Of course, the EXAFS spectrum is analyzed starting from the known parameters for those solid samples whose crystal structure was solved. Interesting information can also be achieved by comparing the experimental spectra of the micellar solution with the theoretical signal of the corresponding crystal structure. Moreover, attempts to fit the solid sample experimental spectra with the MD $g_{Rb,O}(r)$ fitted signal are useful to get valuable information on the Rb^+ coordination in crystals with unknown structure.

Experimental Section

Materials. RbOH is a commercial product (Aldrich). RbDC and RbGDC were prepared by adding a little less than the equivalent amount of a RbOH aqueous solution (Aldrich) to deoxycholic (Calbiochem) and glycodeoxycholic (Sigma) acid, respectively, by filtering the resulting suspensions, and by adding acetone until the solutions became cloudy. RbDC and RbGDC crystals were subsequently grown from the solutions by cooling.[4] RbTDC was prepared by adding $Ba(NO_3)_2$ to an aqueous solution of NaTDC (Sigma). Barium taurodeoxycholate was filtered and crystallized. Subsequently, RbTDC was obtained by adding little more than the equivalent amount of Rb_2SO_4 (Merck, suprapur) to an aqueous suspension of barium taurodeoxycholate and by filtering $BaSO_4$. Finally, RbTDC was twice crystallized from water and acetone.[16]

RbGC was prepared by adding to an aqueous suspension of glycocholic acid a little more than the equivalent amount of RbOH to ensure complete neutralization. RbGC was then precipitated by acetone and twice crystallized from water and acetone.

EXAFS Measurements. The EXAFS spectra above the rubidium K-edge were recorded in the transmission mode at the synchrotrons of Frascati (cRbDC) and HASYLAB-Hamburg. All the measurements were performed at room temperature.

The BX1 beam line of the PWA laboratory (wiggler source, Adone storage ring, Frascati) was equipped with a Si(220) channel cut monochromator and ion chambers with krypton gas filled. The ring was operating at 1.5 GeV with decaying currents from 85 to 10 mA. The ROMO II beam line (bending magnet source, Doris storage ring, Hamburg) was equipped with a Si(311) double crystal monochromator controlled by a special feedback system.[25] The storage ring was running at an energy of 4.45 GeV with an electron current between 40 and 15 mA. The ionization chambers were filled with argon at atmospheric pressure, and a third ionization chamber allowed possible shifts in energy to be checked by recording a reference substance together with the investigated sample.

Molecular Dynamics Computation

The molecular dynamics simulations were performed using an isothermal−isobaric simulation algorithm.[26] Weak coupling to an external temperature bath of 300 K with a coupling time constant of 0.1 ps and to an external pressure bath of 1.0×10^5 Pa with a coupling time constant of 0.5 ps was used to maintain constant temperature and pressure in the simulations. The solute molecules were immersed in cubic boxes containing one Rb^+ ion and 250 water molecules, subjected to periodic boundary conditions. The simulations were performed with programs from the Groningen molecular simulation system (GROMOS) software package.[27] The applied empirical potential energy function contains terms representing bond angle bending, van der Waals, and electrostatic interactions.[28]

The Lennard-Jones parameters of $Rb^+\cdots O$ were those of $Kr\cdots O$ reported by Straatsma et al.[29] The simple point charge (SPC) model was used for water.[30] The SHAKE algorithm was used to constrain bond lengths.[31] The dielectric permittivity was $\epsilon = 1$ and the cutoff distance for the nonbonded interactions was 9 Å. The time step was 2 fs.

All atoms were given an initial velocity obtained from a Maxwellian distribution at the desired initial temperature. After the initial energy minimization of the water molecules, the MD simulations were performed. The first 20 ps were used for equilibration; they were followed by 100 ps that were used for analysis. The trajectories were saved every 50 fs. The calculations were performed on the IBM 3090 of the CASPUR, University of Rome "La Sapienza".

The $g_{Rb,O}(r)$ radial distribution function (left scale) and the running integration number (right scale) are shown in Figure 1. The $g(r)$ presents a first peak with a maximum at 2.93 Å and a minimum region (at about 4.1 Å) where it does not become zero, indicating a not-well-defined solvation shell. At this coordination distance, the running integration number shows the presence of about nine water molecules in the first hydration shell.

EXAFS Calculations

In the present paper we apply the EXAFS analysis on both solid and liquid systems. In the case of a crystalline sample each atom surrounding the photoabsorber contributes to the X-ray absorption cross section with an oscillating signal,[32] and the total $\chi(k)$ contribution can be expressed, as a function of the photoelectron wave vector k, by the equation[33]

$$\chi(k) = \sum_i A(k,r_j) \sin[2kr_j + \varphi(k,r_j)] \qquad (1)$$

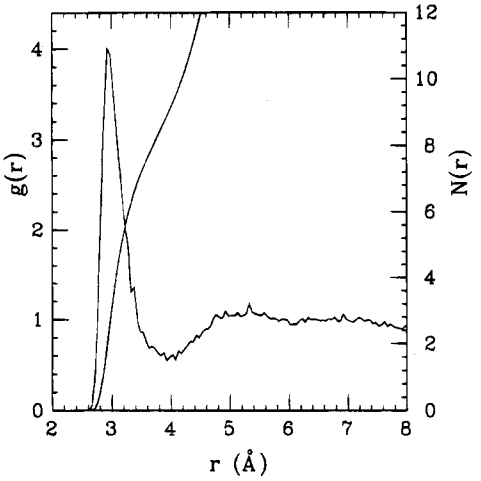

Figure 1. Rb−O radial distribution function as derived from the MD simulations for RbOH water solution (left scale) and corresponding running integration number (right scale).

where $A(k,r_j)$ and $\varphi(k,r_j)$ are the amplitude and the phase function of the jth atom, respectively.

For a liquid system the degree of disorder is larger and, if the photoabsorber is surrounded by a single type of atom, $\chi(k)$ must be represented by the equation

$$\chi(k) = \int_0^\infty dr\, 4\pi\varrho r^2 g(r)\, A(k,r)\, \sin[2kr + \varphi(k,r)] \quad (2)$$

where ϱ is the density of the scattering atoms (atoms/Å^3). The high-distance contribution of the $\chi(k)$ signal is damped by the photoelectron mean-free path $\lambda(k)$ through an exponential function of the type $\exp[-r/\lambda(k)]$ which limits the number of significant terms in eq 1 and leads to an effective upper integration limit of 6−8 Å in eq 2. The mean free path $\lambda(k)$ as well as an additional damping factor accounting for the monochromator resolution are included in the amplitude function.

For the crystalline samples all the structural contributions are calculated with the GNXAS program[34] starting from the known crystal structure. The Rb−O $\chi(k)$ signal of the RbOH aqueous solution is calculated by means of eq 2 starting from the $g_{Rb,O}(r)$ function obtained from the MD simulations. It is worthwhile to stress that the EXAFS signal is extremely sensitive to the short range distances of the $g(r)$ and in particular to the shape of its first rise. By considering the $g(r)$ low-distance shape of several disordered systems, it is evident that the first peak cannot be described by one or more Gaussian functions. A method which employs asymmetric peaks to describe the shape of the $g(r)$ first peak was previously presented.[24] According to this method the MD $g(r)$ first peak is modeled with a Γ-like distribution curve with mean distance R, standard deviation σ, asymmetry index β, and coordination number N_c. This function is used to calculate the first-shell EXAFS contribution. The asymmetric peak is subtracted from the MD $g(r)$, obtaining a long-distance tail whose EXAFS signal is calculated by means of eq 2. This contribution is kept fixed during the minimization, while the four parameters describing the asymmetric peak are refined in order to achieve the best fitting to the experimental spectrum.

Phase shifts are calculated in the muffin-tin approximation starting from overlapped spherically averaged relativistic atomic charge densities. One of the molecular configurations obtained from the MD simulations is used to calculate the phase shifts for the RbOH solution. The muffin-tin radii (R_{MT}) are 1.58 and 1.34 Å for the rubidium and the oxygen atom, respectively.[35] It has been verified that different configurations give the same result. The above mentioned R_{MT} values are used to calculate the rubidium and oxygen phase shifts starting from the RbDC, RbTDC, and RbGC crystal structures. It is found that the rubidium and oxygen phase shift behavior is the same for all the considered systems. R_{MT} values of 0.80 and 0.95 Å are derived for the carbon and sulfur atoms, respectively, in the crystals. A Hedin−Lundqvist plasmon-pole approximation is employed for the self-energy part of the optical potential. The complex potentials allow photoelectron inelastic losses in the final state to be taken intrinsically into account.[36] The known core-hole width[37] (Γ = 2.99 eV) is considered by including a constant factor in the imaginary part of the phase shifts.

The atomic absorption cross section used to extract the EXAFS signal is usually modeled as a smooth function which does not give any structural contribution. Nevertheless, in recent times a careful analysis of the EXAFS spectra of several atomic and molecular systems has revealed the presence of discrete resonances and slope changes in the atomic background, associated with the onset of multielectron excitation channels.[38] Such features can affect the structural analysis of the EXAFS spectra and have to be taken into account in any accurate investigation, as demonstrated for several molecules[39−41] at the Br K-edge.

It was shown that a strong contribution due to multielectron excitations introduces anomalous frequencies in the EXAFS spectra of rubidium at k = 6.0 and 8.6 Å^{-1}, giving rise to low-distance nonstructural peaks in the Fourier transform (FT).[11,42] A first attempt to perform a proper $\chi(k)$ extraction was made by modeling the atomic background on the basis of the absorption spectrum of the krypton gas and by Fourier filtering.[11] Recently, a different background extraction procedure has been proposed and double-electron excitations involving the 1s4s and 1s3d electrons[43,44] have been identified at about 37 and 136 eV above the K-edge, respectively.

In the present work all the spectra are fitted with the FITHEO program[33] including not only the 1s4s and 1s3d double-electron excitation edges, but also the 1s3p edge (namely KN_1, $KM_{4,5}$, and $KM_{2,3}$). According to the $Z + 1$ approximation, the energy onset of the $KM_{2,3}$ channel can be estimated at about 280 eV above the Rb K-edge.[45] The KN_1 and $KM_{2,3}$ edges are modeled with a step-shaped function (see ref 40, eq 3), while the $KM_{4,5}$ threshold presents an edgelike shape which cannot be described by a step-shaped function. The absorption spectrum of the rubidium gas could be employed to perform a satisfactory characterization of this excitation. In the lack of experimental data, we adopt a Lorentzian-shaped function to reproduce the slope change of the atomic background associated with the onset of this excitation channel. Nevertheless, this function is not able to describe the edgelike shape of the $KM_{4,5}$ edge which is visible in all the recorded spectra as a nonstructural peak at about 6.1 Å^{-1}. It is evident that the structural signal is perturbed in this energy region; for this reason the experimental points in a range of about 20 eV around the peak are excluded from the fitting procedure.

For all the spectra the energy position of the KN_1, $KM_{4,5}$, and $KM_{2,3}$ channels is found at 39 ± 5, 136 ± 5, and 281 ± 6 eV from the main edge, respectively, with a step height about 0.3−1.0% of the K-edge jump.

During the fitting procedure three non-structural parameters[39,40] are varied: E_0, which allows the theoretical and experimental scales to be compared, S_0^2, which accounts for the reduced overlap between the passive electrons in the ground-state and in the excited-state relaxed configurations, and δ, which represents the experimental resolution. After the minimization E_0 is found at 2 ± 1 eV from the K-edge, S_0^2 is practically equal to 1, and δ has a value ranging in the interval

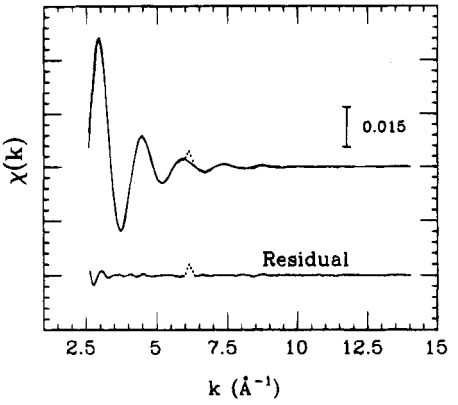

Figure 2. Fit of the RbOH aqueous solution experimental spectrum. Experimental spectrum compared with the $\chi(k)$ fitted signal calculated from the MD $g_{Rb,O}(r)$, and the residual. The dots represent the experimental points excluded from the fitting.

3.2−3.6 eV, depending on the experimental setup used in the measurements.

Results and Discussion

The main contribution to the X-ray absorption cross section of a 0.2 M RbOH aqueous solution is due to the Rb−O pair correlation function. The Rb−O EXAFS signal is calculated by means of eq 2 using the $g_{Rb,O}(r)$ obtained from the MD simulations. This method allows the reliability of the $g(r)$ distribution function to be checked, on the one hand, and the water signal to be properly calculated, on the other. In Figure 2 we report the comparison between the fitted $\chi(k)$ signal and the experimental spectrum, together with the residuals. The fitting is performed in the range $2.5 \leq k \leq 14$ Å^{-1} and dots around $k = 6.1$ Å^{-1} represent the experimental points excluded from the minimization. The agreement between theory and experiment is excellent with the exception of the low-k region. This behavior can be due both to the muffin-tin approximation, which is less reliable in this region, and to the presence of the KN_I edge, which could affect the correct extraction of the $\chi(k)$ signal. The fit index, as defined by eq 5 of ref 40, is $R_i = 0.135 \times 10^{-6}$. A rough estimate of the free parameters that can be fitted is given by the $2\Delta k\Delta r/\pi$ rule[46] which supports the present least-squares fitting procedure. Δk is the k-space range over which the $\chi(k)$ signal is fitted and Δr is the width of the r-space Fourier filter window. In our case Δk is about 11.5 Å^{-1} and Δr is limited by the mean-free path only, since we are not Fourier filtering the data. From the fitting procedure a $g_{Rb,O}(r)$ shift of about 0.1 Å to shorter distances is observed. This could be ascribed to the semiempirical potentials employed and/or to the absence of a hydrogen-bonding potential function in the MD simulations. As shown in the previous section the EXAFS analysis is also performed by describing the $g(r)$ first peak with an asymmetric shell and the remaining solvent contribution with the $g(r)$ long-distance tail. The results of this analysis are reported in Figure 3. Starting from the top, the asymmetric peak contribution, the tail signal, their sum compared with the experimental spectrum, and the residuals are shown. In this case the Rb^+ ion does not present a well defined first solvation shell, and therefore the tail contribution to the EXAFS spectrum is expected to be significant. By looking at the tail signal, it is evident that its inclusion is essential to reproduce the experimental spectrum, especially in the low-k region. The refined parameters, obtained from the fitting procedure, are $R = 3.20 \pm 0.01$ Å, $\sigma = 0.394 \pm 0.008$Å^{-1}, $\beta = 1.47 \pm 0.05$, and $N_c = 8.5 \pm 0.5$ (the fit index is 0.124×10^{-6}). In Figure 4 we report the asymmetric peak after the minimization, compared with the MD $g(r)$. Also in this case

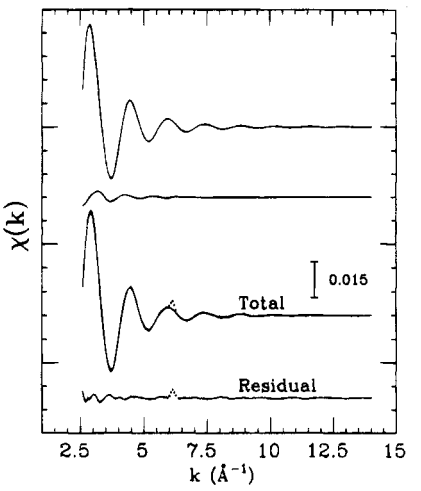

Figure 3. Fit of the RbOH aqueous solution experimental spectrum. From top to bottom are reported the asymmetric peak $\chi(k)$ contribution, the tail signal, their sum compared with the experimental spectrum, and the residual.

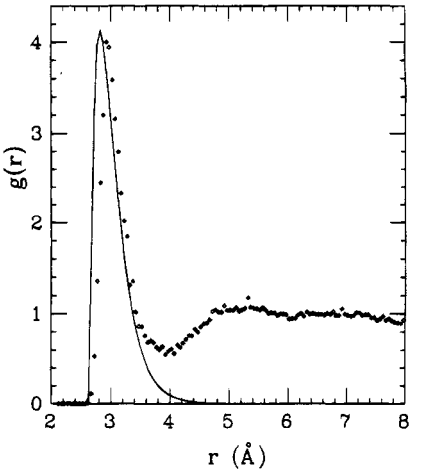

Figure 4. Asymmetric peak obtained from the EXAFS analysis compared with the $g_{Rb,O}(r)$ obtained from the MD simulations.

the first peak obtained from the EXAFS analysis is slightly shifted to shorter distances with respect to the MD $g(r)$.

Provide a deeper insight into the Rb^+ coordination in aqueous solutions, it is interesting to report previous results obtained from EXAFS[11,47,48] and differential anomalous scattering (DAS) measurements.[47] In particular for a 4.6 M RbBr aqueous solution a Rb−O distance shell of 2.9 and 2.84 Å was determined by means of DAS and EXAFS measurements, respectively.[47] From the EXAFS results, a Gaussian shell width of 0.161 Å was found and no evidence of additional coordination shells was pointed out. Due to disorder effects, the coordination number was not determined. EXAFS measurements of RbBr aqueous solutions at concentrations ranging between 1 and 6 M were presented in a more recent paper.[48] The water molecule asymmetric radial distribution was approximated by two symmetric Gaussian functions. The average values found for the two shells were 2.83, 2.93 Å and 3.2, 3.6 for the distances and coordination numbers, respectively. The values of the first and second shell width were found in the ranges 0.072−0.163 Å and 0.066−0.200 Å, respectively.

For a 0.15 M rubidium oxalate solution two pairs of Gaussian shells were used with the following parameters: 2.71, 2.84, 3.72, 4.05 Å, 2.3, 3.9, 4.0, 4.0, and 0.128, 0.132, 0.134, 0.145 Å for the distances, coordination numbers and shell widths, respectively.[11] The necessity to reproduce both the asymmetric water radial distribution and the tail contribution can account for the

TABLE 1: cRbDC Refined Parameters[a]

T	N[b]	R (Å)	DW (Å^2)
O	0.5	2.65	0.004
O	2.0	2.87	0.015
O	5.0	2.91	0.017
O	4.5	3.05	0.035
O	5.0	3.13	0.038
O	0.5	3.28	0.009
O	5.0	3.37	0.026
O	1.0	3.56	0.010
O	2.0	3.68	0.006
O	5.0	3.90	0.037
C	1.0	3.41	0.024
C	1.0	3.54	0.010
C	1.0	3.63	0.007
C	1.0	3.81	0.004
Rb	2.0	3.81	0.036

[a] T and N indicate the atomic type and the number of atoms, respectively, R is the coordination distance, and DW is the Debye–Waller factor (σ^2). [b] The coordination numbers are weighted $^1/_3$ for each shell.

use of two pairs of Gaussian shells. By considering the first three shells a total of 10.2 water molecules was found, which is 1.19 times greater than the $g(r)$ running integration number up to 3.85 Å (third distance shell plus σ) obtained from our analysis.

In the present work the refined $g(r)$ obtained from the EXAFS analysis of the RbOH aqueous solution is used as a coordination model for the micellar solutions. In particular, by comparing the refined EXAFS signal of the MD $g(r)$ with the micellar solution spectra it is possible to point out whether the Rb^+ coordination in the micellar systems is equal to or different from that in water.

An EXAFS study of the crystal and a 0.3 M micellar solution of RbDC was previously accomplished.[11] In the present work an advanced data analysis method (GNXAS package[34]) is applied in order to perform a coherent analysis of both the RbDC and the other rubidium bile acid salt spectra.

The RbDC crystal has three independent Rb^+ ions in the asymmetric unit with a very irregular coordination, which cannot be simulated by a low number of coordination shells. The cRbDC theoretical signal is calculated starting from the crystal structure.[4] All the contributions with half path length $\leq$ 4.0 Å are considered and grouped in 15 shells, containing also Rb^+ ions and carbon atoms, at variance with the previous analysis.[11] Six shells contain only one contact. During the minimization, the shell distances are varied within a narrow range (±0.08 Å) around the starting values in order to account for the indetermination arising from the shell choice. The coordination numbers of each shell (weighted $^1/_3$ for each independent Rb^+ ion) are kept fixed. To get the best agreement between the calculated and experimental data we also vary the Debye–Waller factor (DW) for each path. The refined parameters of each shell are reported in Table 1. The refined distances of the shells with only one scattering atom present a maximum shift of ±0.04 Å. The wide range of DW values found for different shells can be explained in most cases as an effect of grouping atoms. In principle, it is possible to obtain information on the DW values from the solution of the crystal structures, which provide the atomic temperature factors. However, the low number of collected reflections used in the solution of RbDC crystal structure (and also in the case of RbTDC and RbGC) causes high and meaningless atomic temperature factors. This does not allow us to compare the DW fitted values with the mean-square amplitudes of vibration deduced from the crystal structure data. As an example, we can mention the case of the shells with no grouped atoms. The mean-square amplitudes of vibration of the Rb^+ ions, taken over the joint distribution of

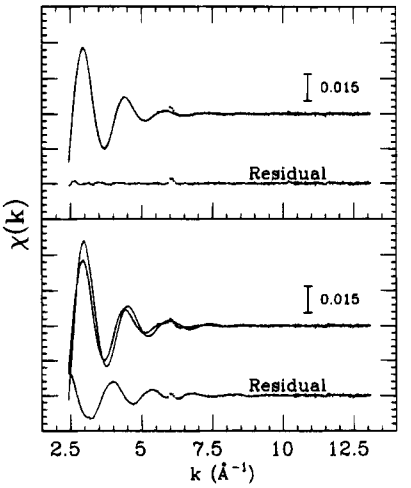

Figure 5. Fit of the cRbDC experimental spectrum. Upper panel: the $\chi(k)$ total theoretical signal calculated for the Rb^+ coordination in the RbDC crystal compared with the experimental spectrum, and the residual. Lower panel: the $\chi(k)$ theoretical signal calculated from the MD $g_{Rb,O}(r)$ compared with the experimental spectrum, and the residual.

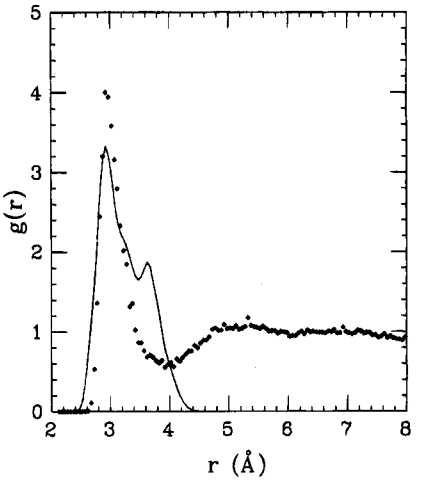

Figure 6. Comparison of the refined MD $g(r)$ with the MD $g(r)$ of cRbDC, obtained by summing the Gaussian shells reported in Table 1.

the pairs, are varying between 0.207 and 0.532 Å^2. The experimental structural signal, compared with the total theoretical contribution, and the residual curve are reported in the upper panel of Figure 5. The agreement between the experimental and the theoretical signals is excellent ($R_i = 0.315 \times 10^{-5}$), and the residual contains only statistical noise. Also in this case some experimental points in the energy region of the $KM_{4,5}$ edge are excluded from the fitting. It is important to mention that for the EXAFS analysis of the cRbDC we start from a known coordination. For each shell, only the DW factor is free to vary, and the fit is obtained from a restrained refinement, with a reduced number of structural parameters.

To verify the existence of a different Rb^+ coordination in the crystal and in the RbOH aqueous solution, we have tried to fit the cRbDC spectrum with the $\chi(k)$ refined theoretical signal obtained from the MD $g_{Rb,O}(r)$. During the minimization the theoretical structural contribution is kept fixed, and the $\chi(k)$ signal is extracted using the same background parameters (spline and double-excitation functions) of the previous analysis. The results are reported in the lower panel of Figure 5. In this case the agreement between experiment and theory is unsatisfactory, and the residuals present a strong oscillation with the typical frequency of the structural contribution. By releasing all the parameters, the agreement is not improved. In Figure 6 a comparison of the refined MD $g(r)$ with the $g(r)$ of cRbDC,

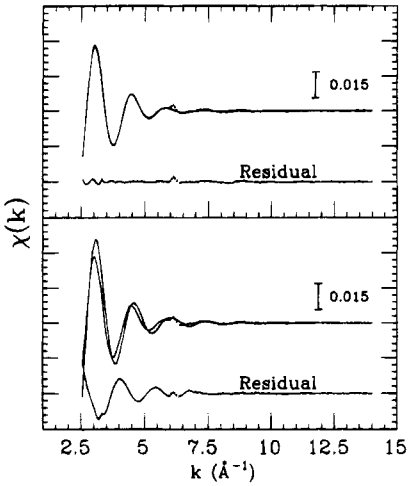

Figure 7. Fit of the sRbDC experimental spectrum. Upper panel: the $\chi(k)$ total theoretical signal calculated for the Rb^+ coordination in the RbDC crystal compared with the experimental spectrum, and the residual. Lower panel: the $\chi(k)$ theoretical signal calculated from the MD $g_{Rb,O}(r)$ compared with the experimental spectrum, and the residual.

obtained by summing the Gaussians reported in Table 1 is shown. The difference between the two $g(r)$ in the r-space of the crystal demonstrates that the Rb^+ coordination in the crystal and in the RbOH solution is different. Therefore, the EXAFS technique seems to be suitable to focus differences in the Rb−O coordination.

The next step is the analysis of the sRbDC (0.3 M) EXAFS spectrum. The same procedure used for the crystal is applied to the micellar solution. First, the fitting of the sRbDC spectrum is done starting from the crystal refined parameters reported in Table 1. After the minimization, the mean of the distance variations is 0.02 Å. Most of the DW are found to be greater than those of Table 1, with a mean value of 0.01 $Å^2$. This change is easily justified by an increment of disorder in the RbDC micellar structure, as compared with the crystalline one. Second, the $\chi(k)$ signal obtained from the refined MD $g_{Rb,O}(r)$ is compared with the experimental spectrum. In both cases, the parameters describing the atomic background are moved during the minimization. Differences in the shape of the double-excitation edges can occur owing to the different absorption background of the crystal and of the micellar solution. Nevertheless, only small changes of the parameters describing the excitation edges are found after the minimization. In Figure 7 the comparison of the sRbDC experimental spectrum with the crystal (upper panel) and $g(r)$ (lower panel) theoretical signals is shown, together with the residuals. The agreement between experiment and theory is good in the former case ($R_i = 0.135 \times 10^{-6}$), while is unsatisfactory in the latter ($R_i = 0.244 \times 10^{-5}$). Notice that the residuals reported in the lower panels of Figures 5 and 7 present quite a similar oscillation frequency, indicating a close resemblance of the RbDC crystal and micellar solution spectra. This investigation, performed with a new EXAFS analysis method, confirms the results previously published[11] for the RbDC helical system.

A less clear picture emerges from the experimental data available for the conjugated salts of deoxycholic acid. The crystal structures of the salts solved so far allow three types of helices to be identified, namely 6_5, 3_1, and 2_1 helices.[9,15,16] However, helical fibers of NaTDC, RbTDC, NaGDC, and RbGDC are reasonably formed by structural units closer to those of the micellar aggregates than those observed in the crystals, since their fibers can be drawn directly from the aqueous micellar solutions by increasing, for example, the ionic strength. Unfortunately, the 6_5, 3_1, and 2_1 helices do not satisfy the X-ray data collected for the fibers and, therefore, a different helix is

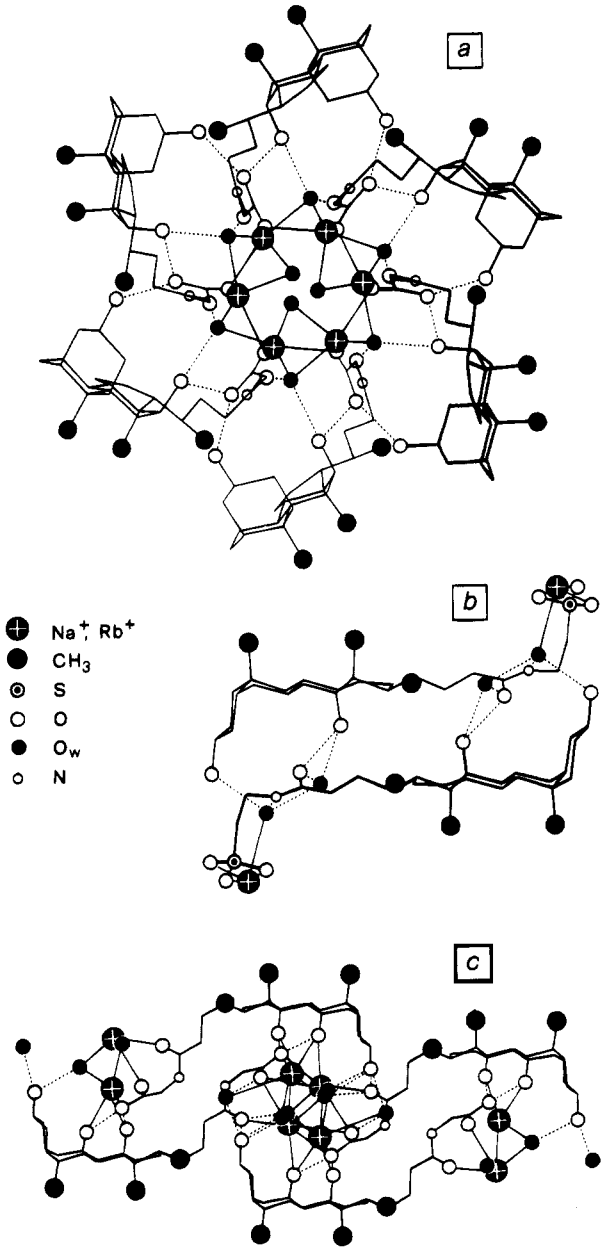

Figure 8. (a) NaGDC helix projected along the 6_5 helical axis. (b) One of the two helices observed in the RbTDC crystal projected along the 2_1 helical axis. (c) RbGC bilayer projected along 2-fold rotation axes. A thick line represents an anion nearer to the observer. Dotted and thin full lines represent hydrogen bonding and ion−ion or ion−dipole interactions, respectively.

present in all four fibers, since their X-ray patterns, unit cell constants, and helical parameters are nearly equal.[16,23] The analysis of the X-ray data pointed out that the structural unit is a 7/1 helix with a radius and a periodicity along the helical axis of about 10 and 45 Å, respectively, the repetitive unit consisting of three salt and some water molecules (a trimer). Strong evidence that the trimer is stable in aqueous solution and that, hence, the 7/1 helix can represent adequately the structure of the micellar aggregate comes from electromotive force measurements of galvanic cells, containing electrodes reversible to sodium, hydrogen, glycodeoxycholate,[49] or taurodeoxycholate[50] ions, accomplished as a function of pH, ionic strength, and bile salt concentration. Significant concentrations of trimeric species were detected, and in the case of NaTDC the most part of the micellar aggregates have, astonishingly, aggregation numbers multiples of three higher for NaTDC and $N(CH_3)_4Cl$ concentrations up to 0.06 and 0.40 M, respectively, and pH values ranging from 7 to 10. However, all these results

TABLE 2: cRbTDC Refined Structural Parameters[a]

T	N[b]	R (Å)	DW (Å^2)
O	1.0	2.85	0.005
O	3.0	2.94	0.022
O	4.0	2.98	0.055
O	2.0	3.10	0.055
O	4.0	3.29	0.055
O	1.0	3.43	0.005
O	1.0	3.78	0.010
S	3.0	3.69	0.054
S	2.0	3.80	0.055
S	2.0	4.08	0.025
C	1.0	3.59	0.016
C	3.0	3.92	0.058

[a] The symbols have the same meaning as in Table 1. [b] The coordination numbers are weighted $^1/_2$ for each shell.

are insufficient to infer a clearly defined structural model. The helical radius of about 10 Å is in agreement with that of the NaGDC 6_5 helix observed in the crystal[9] (Figure 8a) and, therefore, the 7/1 helix could be derived from the 6_5 one. On the other hand, we did not succeed in solving the structure of a RbGDC monoclinic crystal (space group $C2$), since the ratio number of reflections/number of positional and thermal parameters is too low. Thus, it was decided to resort to the EXAFS technique to get more enlightening information and to answer the following questions. The first question regards the possibility of using the 6_5 helix of NaGDC as a starting model from which the 7/1 helix, proposed as a representative model of the micellar aggregates, can be obtained by small adjustments. This is possible only if the Rb^+ coordination in the micellar aqueous solutions is different from that of Rb^+ in water, since the counterions are firmly anchored inside the NaGDC helix, as in the case of RbDC and NaDC, and have a peculiar coordination. The second question regards the 7/1 helix that can represent the glyco- and taurodeoxycholate micellar aggregates only if their EXAFS spectra are similar. The third question regards the possibility that some micellar aggregates are 2_1 helices or bilayers as those observed in the crystal structures of the triclinic NaTC[18] and monoclinic RbTDC[16] and RbGC[20] (Figure 8b,c). A comparison between the spectrum of a crystal, formed by the packing of 2_1 helices or bilayers, and that of an aqueous micellar solution can be conclusive.

The crystal packing of a RbTDC monoclinic phase[16] is characterized by hydrophilic and hydrophobic channels, both centered on 2-fold rotation axes. The hydrophilic channel is filled with rubidium and sulfonate ions and water molecules. Two pairs of two different helices with twofold screw axes are arranged around this channel. The helices are mainly held together by ion−ion interactions, involving the sulfonate and rubidium ions, and by hydrogen bonds. The asymmetric unit contains two nonequivalent rubidium ions heptacoordinated with the oxygens of the sulfonate groups and, only for one of them, with one water and one hydroxyl oxygen. The Rb^+ ions are located in the outer surface of the helices (see Figure 8b).

The EXAFS analysis of this RbTDC crystal phase is performed starting from two clusters (weighted $^1/_2$) describing the coordination of the two nonequivalent Rb^+ ions in the RbTDC crystal structure. The distances are grouped in 12 shells, 4 of them containing only one contact. The theoretical signal corresponding to each coordination shell is calculated and the distances together with the DW factors are refined in order to achieve the best agreement with the experimental spectrum. The structural parameters, reported in Table 2, are obtained from the least-squares method moving the coordination distances in a narrow range (±0.07 Å) around the starting values. In the upper panel of Figure 9 we report the total theoretical contribution compared with the experimental signal and the residual. The agreement between theory and experiment is satisfactory ($R_i = 0.122\times 10^{-7}$). By looking at the refined distances of shells with only one scattering atom the reliability of the crystalline structure can be partially verified. The mean distance shift is −0.01 Å, with a maximum of 0.05Å.

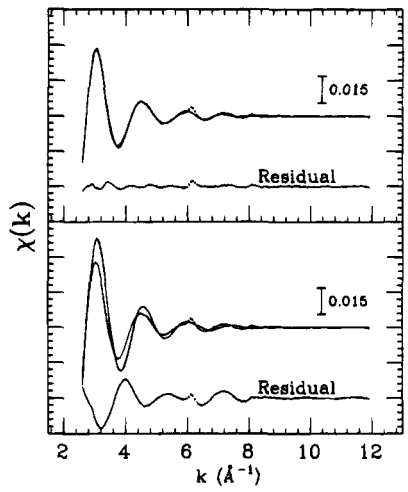

Figure 9. Fit of the cRbTDC experimental spectrum. Upper panel: the $\chi(k)$ total theoretical signal calculated for the Rb^+ coordination in the RbTDC crystal compared with the experimental spectrum, and the residual. Lower panel: the $\chi(k)$ theoretical signal calculated from the MD $g_{Rb,O}(r)$ compared with the experimental spectrum, and the residual.

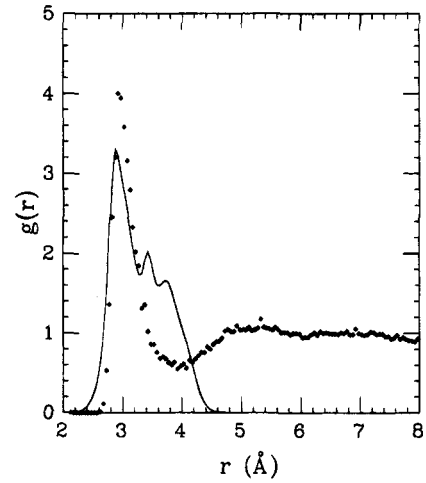

Figure 10. Comparison of the refined MD $g(r)$ with the MD $g(r)$ of cRbTDC, obtained by summing the Gaussian shells reported in Table 2.

The difference between the sum of Gaussians reported in Table 2 and the refined MD $g(r)$, shown in Figure 10, indicates the existence of significant differences between the Rb^+ coordination in the crystal and in water. The cRbTDC $\chi(k)$ experimental spectrum is compared with the refined MD $g(r)$ theoretical signal in the lower panel of Figure 9. The strong oscillation in the residual allows a significatively different Rb^+ coordination in the crystal and in the aqueous solution to be assessed. The sulfonate groups give rise to additional Rb−S signals with different amplitude and phase shift with respect to the Rb−O contributions. The Rb−S distances, together with a different Rb-O coordination, account for the strong disagreement between theory and experiment visible in the lower panel of Figure 9. No improvement is obtained with an iterative refinement.

A peculiar Rb^+ coordination in the RbTDC micellar solution (0.2 M) is checked by comparing the sRbTDC spectrum with the $g_{Rb,O}(r)$ calculated one. The experimental and calculated signals together with the residual are shown in Figure 11. The

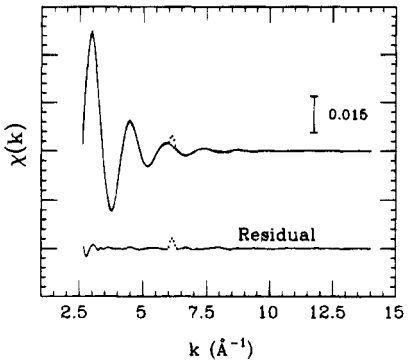

Figure 11. Fit of the sRbTDC experimental spectrum. The $\chi(k)$ theoretical signal calculated from the MD $g_{Rb,O}(r)$ compared with the experimental spectrum, and the residual.

agreement between the two curves is excellent, indicating a very similar Rb^+ coordination in the RbTDC micellar and RbOH aqueous solutions. After the minimization, the refined MD $g(r)$ gives rise to a shift of 0.016 Å and a fit index $R_i = 0.759 \times 10^{-7}$. From these results it is possible both to discard the 2_1 helices of the RbTDC crystal (Figure 8b) as a model for the micellar aggregates and to infer that the Rb^+ ions should have a liquidlike coordination. However, it must be stressed that the size of the RbTDC micellar aggregates in aqueous solutions without added salt (RbCl) is small[23] and, therefore, only the trimers and the oligomers, some of which are probably constituted by a few trimers, have the Rb^+ ions with a liquidlike coordination. Of course, the Rb^+ coordination could change in the 7/1 helix. In this connection it must be noticed that the NaTDC micellar aggregates in salt solutions resulted in their becoming highly hydrated on the basis of sedimentation and diffusion measurements.[51] An EXAFS study of the RbTDC fibers and micellar solutions at high ionic strength could give more information on the RbTDC micellar structure.

As far as the NaGDC micellar aggregates are concerned, a helical model in solution was supported by CD measurements and energy calculations.[9] The observed preferential interaction of the NaGDC micellar aggregates with the left-handed BR molecule indicated a chiral structure of the micelle. Unfortunately, the RbGDC crystal structure is unknown, but the helical model proposed for NaGDC can be extended also to the RbGDC micellar aggregates on the basis of their very similar X-ray fiber patterns and quasielastic light scattering (QELS) data, collected as a function of ionic strength, concentration and temperature.[23] However, the size of the micellar aggregates in aqueous solution without NaCl or RbCl is small as in the case of NaTDC and RbTDC. The MD $g_{Rb,O}(r)$ is used as a Rb^+ coordination model both for the RbGDC crystal and micellar solution (0.2 M). The experimental spectra are compared with the refined $\chi(k)$ signal calculated from the $g_{Rb,O}(r)$, and the background parameters are refined while the structural signal practically does not change. The results of this analysis are reported in Figure 12. Both the cRbGDC and sRbGDC experimental spectra (upper and lower panel, respectively) are well reproduced by the theoretical signal. The values of the fit index are 0.397×10^{-7} and 0.266×10^{-6}, respectively. In the case of cRbGDC the agreement between the experimental spectrum and the calculated signal indicates a Rb^+ coordination like that of an amorphous material. This finding could be due to disorder that can account for the low number of observed reflections and, hence, the failure to solve the crystal structure. In conclusion, even though the RbGDC crystal structure was known, the lack of a peculiar coordination in the crystal on one hand and the similarity of the cRbGDC, sRbGDC, and RbOH spectra on the other does not allow a model of the RbGDC micellar aggregates to be established. Nevertheless, the similar disordered Rb^+ coordination in the

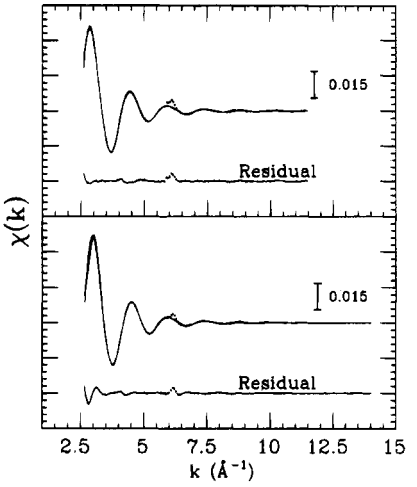

Figure 12. Upper panel: the cRbGDC experimental spectrum compared with the MD $g_{Rb,O}(r)$ theoretical signal, and the residual. Lower panel: the sRbGDC experimental spectrum compared with the MD $g_{Rb,O}(r)$ theoretical signal, and the residual.

RbGDC and RbTDC micellar solutions, evidenced by the EXAFS data, is not in disagreement with a similar structure of the glyco- and taurodeoxycholate micellar aggregates. Moreover, the 6_5 helix of the NaGDC crystal can be rejected as approximate model for the 7/1 helix. Since most of the Rb^+ ions in a small aggregate can be approached by the water molecules of the solvent, small micellar aggregates with the structure of the 6_5 helix can present a Rb^+ coordination which could result different from that of the 6_5 helix. However, this is unlikely since the small aggregates of RbDC, investigated under conditions nearly equal to those of RbGDC and RbTDC, have a structure similar to that of the 6_5 helix and show a similar coordination of the Rb^+ ions in the crystal, fiber, and aqueous micellar solution,[11] at variance with the behavior of RbGDC and RbTDC.

It is well-known that aqueous micellar solutions of trihydroxy and dihydroxy bile salts show a different behavior.[1] Several examples can be provided supporting, at least, two different types of micellar structures. Among the others, it is worthwhile to mention the following:

(i) An electron spin resonance study which showed the coexistence of a strongly and a weakly immobilized component in the case of some dihydroxy bile salts (NaDC, NaTDC, sodium taurochenodeoxycholate, and sodium tauroursodeoxycholate), while only the weakly immobilized component is present in the case of the trihydroxy bile salts (NaTC and sodium cholate).[52]

(ii) A QELS study on aqueous micellar solutions of NaGDC, RbGDC, NaTDC, RbTDC, NaGC, RbGC, NaTC, and RbTC which showed once more that the behavior of the dihydroxy salts differs significantly from that of the trihydroxy ones when the ionic strength is increased and that the dihydroxy salts on one hand and the trihydroxy ones on the other behave likewise.[23]

(iii) A CD study of the interaction complexes between BR and NaDC,[7] NaTDC, RbTDC,[16] NaGC, and NaTC[19] which showed a close resemblance between the spectra of the dihydroxy salts on one hand and of the trihydroxy ones on the other.[16] Furthermore, the spectra recorded as a function of the ionic strength of the dihydroxy salts remarkably differ from those of the trihydroxy ones, suggesting that the chiral recognition of BR is sensitive to the structure of the micellar aggregates.

Thus, it is interesting to compare the EXAFS spectrum of the trihydroxy RbGC with those of the dihydroxy RbTDC and RbGDC, bearing in mind that the above-mentioned dihydroxy and trihydroxy salts without NaCl or RbCl give rise to similar

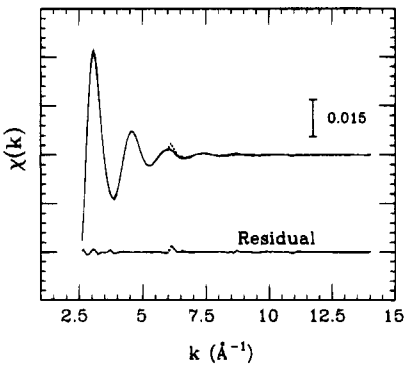

Figure 13. Fit of the cRbGC experimental spectrum. The $\chi(k)$ total theoretical signal calculated for the Rb^+ coordination in the RbGC crystal compared with the experimental spectrum, and the residual.

TABLE 3: cRbGC Refined Structural Parameters[a]

T	N[b]	R (Å)	DW (Å²)
O	1.0	2.72	0.005
O	3.0	2.87	0.010
O	3.0	2.99	0.080
O	2.0	3.47	0.054
O	2.0	3.80	0.073
O	4.0	4.03	0.058
C	5.0	3.70	0.048
C	2.0	3.96	0.079
Rb	2.0	4.25	0.030

[a] The symbols have the same meaning as in Table 1. [b] The coordination numbers are weighted $^1/_2$ for each shell.

QELS data corresponding to small aggregates. Crystals of RbGC, belonging to the $C2$ space group, are taken into account.[20] They are characterized by one Rb^+ ion, located in two sites with occupancy factor $^1/_2$, in the asymmetric unit and by a packing of bilayers (Figure 8c). The EXAFS spectra of cRbGC and sRbGC are analyzed in order to get information on the Rb^+ coordination of the RbGC micellar solution (0.2 M).

The same procedure described for the other samples is applied also in this case. The cRbGC experimental spectrum is reproduced starting from the known Rb^+ coordination in the crystal structure by grouping the atoms in nine shells. By looking at the results of this analysis reported in Figure 13, a good agreement between the calculated and the experimental spectrum is observed. The refined coordination parameters obtained from the minimization ($R = 0.133 \times 10^{-6}$) are given in Table 3. As in the previous cases, a comparison of the Rb^+ coordination both in the crystal and in solution is performed by fitting the cRbGC and sRbGC spectra with the $\chi(k)$ signal calculated for $g_{Rb,O}(r)$. In the upper panel of Figure 14 the experimental cRbGC spectrum, the calculated signal, and the residual are shown. The presence of a structural signal in the residual is evident. We can deduce that the Rb^+ coordination in the cRbGC is different from that in water by comparing the amplitude of the oscillations present in the residual with that of the residuals of cRbDC (Figure 5) and cRbGDC (upper panel of Figure 12), which show a strong structural signal and a quite flat signal, respectively. This result accounts for the difference between the refined MD $g(r)$ and the sum of the Gaussians reported in Table 3, as shown in Figure 15.

The sRbGC spectrum is in agreement with the Rb^+ coordination in water ($R_i = 0.114 \times 10^{-5}$), as shown in the lower panel of Figure 14. The oscillation present in the residual at low k is not enough marked to justify a peculiar coordination in the micellar solution of RbGC and, therefore, the Rb^+ coordination inside the bilayer (Figure 8c) can be discarded. These results, together with those of sRbTDC and sRbGDC, seem to indicate

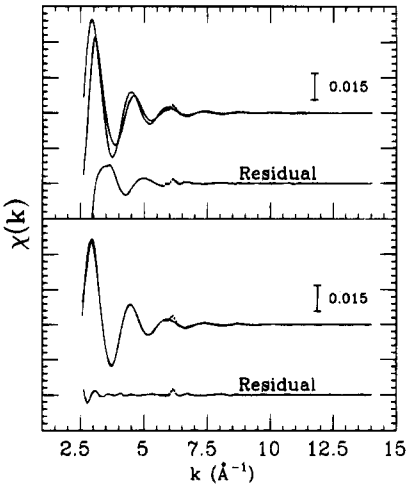

Figure 14. Upper panel: the cRbGC experimental spectrum compared with the MD $g_{Rb,O}(r)$ theoretical signal, and the residual. Lower panel: the sRbGC experimental spectrum compared with the MD $g_{Rb,O}(r)$ theoretical signal, and the residual.

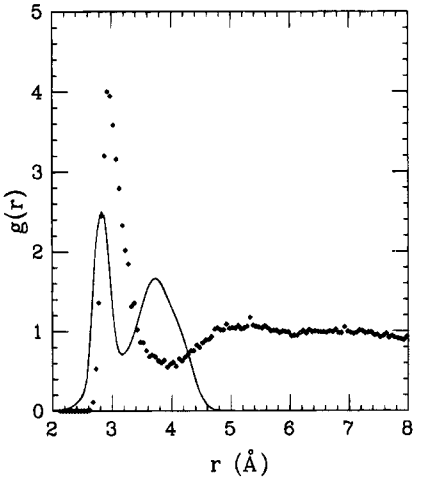

Figure 15. Comparison of the refined MD $g(r)$ with the MD $g(r)$ of cRbGC, obtained by summing the Gaussian shells reported in Table 3.

that the small aggregates have the Rb^+ ions either exposed to the water molecules of the solvent or dipped into the bulky solvent.

Conclusions

The most important results of this study can be summarized as follows:

(i) The Rb−O pair distribution function obtained from MD simulations has been successfully refined by using the EXAFS spectrum of a dilute RbOH solution. This result points out that EXAFS measurements can give an appropriate description of the local disordered environment around the excited atom if radial distribution functions or asymmetric peaks are employed in the calculations. Moreover, calculated X-ray absorption spectra, directly fitted with the raw experimental data, and modeled background spectra, accounting for the double-excitation edges, allow an accurate EXAFS analysis to be performed.

(ii) The refined $g_{Rb,O}(r)$ represents a suitable model for the Rb^+ solvated ion. The present work demonstrates the successful use of this model in order to distinguish a characteristic coordination from a disordered one in crystals and micellar systems of bile acid salts as RbDC, RbTDC, RbGDC, and RbGC. When the crystal structure is unknown or the crystals are inadequate to collect good X-ray diffraction data, the crystalline powder EXAFS measurements allow one to easily

search regular or peculiar coordinations and to get information on the change between the coordination in water and in the crystal.

(iii) The EXAFS measurements carried out on crystals and aqueous solutions of rubidium salts containing micellar aggregates of small size, provide the following results. The Rb^+ ions of RbDC have a very similar coordination in the crystal and in the aqueous micellar solution. The Rb^+ ions of sRbGDC, sRbTDC, and sRbGC are coordinated as those of RbOH in water. The 6_5 and 2_1 helices and the bilayer can be discarded as representative models of these micellar aggregates. Moreover, these results are not in disagreement with those inferred from the X-ray diffraction patterns, which provide the same model (the 7/1 helix) for both RbGDC and RbTDC micellar aggregates.[16]

Acknowledgment. The authors would like to acknowledge the hospitality and technical assistance of the HASYLAB (Hamburg) and in particular Dr. Peter Kizler for his personal support and invaluable technical help. Thanks are due to Drs. L. Galantini, E. Gavuzzo, and L. Scaramuzza for providing atomic coordinates of the RbGC crystal structure prior to publication. This work was sponsored by the Italian Consiglio Nazionale delle Ricerche and by the Italian Ministero per l'Università e per la Ricerca Scientifica e Tecnologica.

References and Notes

(1) Small, D. M. In *The Bile Acids*; Nair P. P., Kritchevsky, D., Eds.; Plenum: New York, 1971, Vol 1. Carey, M. C. In *Bile Acids in Gastroenterology*; Barbara L., Dowling, R. H., Hofmann, A. F., Roda, E., Eds.; MTP Press: Boston, 1983. Carey M. C. In *Sterols and Bile Acids*; Danielsson, H., Sjövall, J., Eds.; Elsevier North-Holland Biomedical Press: Amsterdam, 1985.

(2) Conte, G.; Di Blasi, R.; Giglio, E.; Parretta, A.; Pavel, N. V. *J. Phys. Chem.* **1984**, *88*, 5720.

(3) Campanelli, A. R.; Ferro, D.; Giglio, E.; Imperatori, P.; Piacente, V. *Thermochim. Acta* **1983**, *67*, 223.

(4) Campanelli, A. R.; Candeloro De Sanctis, S.; Giglio, E.; Petriconi, S. *Acta Crystallogr., Sect. C* **1984**, *40*, 631.

(5) Esposito, G.; Giglio, E.; Pavel, N. V.; Zanobi, A.; Campbell, I. D. *J. Phys. Chem.* **1987**, *91*, 83.

(6) Chiessi, E.; D'Alagni, M.; Esposito, G.; Giglio, E. *J. Inclusion Phenom. Mol. Recognit. Chem.* **1991**, *10*, 453.

(7) D'Alagni, M.; Delfini, M.; Galantini, L.; Giglio, E. *J. Phys. Chem.* **1992**, *96*, 10520.

(8) D'Alagni, M.; Forcellese, M. L.; Giglio, E. *Colloid Polym. Sci.* **1985**, 263, 160.

(9) Campanelli, A. R.; Candeloro, De Sanctis, S.; Chiessi, E.; D'Alagni, M.; Giglio, E.; Scaramuzza, L. *J. Phys. Chem.* **1989**, *93*, 1536.

(10) Esposito, G.; Giglio, E.; Pavel, N. V.; Zanobi, A. *J. Phys. Chem.* **1987**, *91*, 356.

(11) Giglio, E.; Loreti, S.; Pavel, N. V. *J. Phys. Chem.* **1988**, 92, 2858.

(12) Burattini, E.; D'Angelo, P.; Giglio, E.; Pavel, N. V. *J. Phys. Chem.* **1991**, *95*, 7880.

(13) Ascone, I.; D'Angelo, P.; Pavel, N. V. *J. Phys. Chem.* **1994**, *98*, 2982.

(14) Bottari, E.; Festa, M. R.; Jasionowska, R. *J. Inclusion Phenom. Mol. Recognit. Chem.* **1989**, *7*, 443.

(15) Campanelli, A. R.; Candeloro, De Sanctis, S.; Giglio, E.; Scaramuzza, L. *J. Lipid Res.* **1987**, *28*, 483.

(16) D'Alagni, M.; D'Archivio, A. A.; Giglio, E.; Scaramuzza, L. *J. Phys. Chem.* **1994**, *98*, 343

(17) Campanelli, A. R.; Candeloro De Sanctis, S.; Galantini, L.; Giglio, E.; Scaramuzza, L. *J. Inclusion Phenom. Mol. Recognit. Chem.* **1991**, *10*, 367.

(18) Campanelli, A. R.; Candeloro De Sanctis, S.; D'Archivio, A. A.; Giglio, E.; Scaramuzza, L. *J. Inclusion Phenom. Mol. Recognit. Chem.* **1991**, *11*, 247.

(19) D'Alagni, M.; Galantini, L.; Giglio, E.; Gavuzzo, E.; Scaramuzza, L. *J. Chem. Soc., Faraday Trans.* **1994**, *90*, 1523.

(20) D'Archivio, A. A.; Galantini, L.; Gavuzzo, E.; Giglio, E.; Scaramuzza, L., unpublished results.

(21) Cobbledick, R. E.; Einstein, F. W. B. *Acta Crystallogr.* **1980**, *B36*, 287.

(22) Coiro, V. M.; Giglio, E.; Morosetti, S.; Palleschi, A. *Acta Crystallogr.* **1980**, *B36*, 1478.

(23) Briganti, G.; D'Archivio A. A.; Galantini L.; Giglio E., unpublished results

(24) D'Angelo, P.; Di Nola, A.; Filipponi, A.; Pavel, N. V.; Roccatano, D. *J. Chem. Phys.* **1994**, *100*, 985.

(25) Krolzig, A.; Materlik, G.; Swars, M.; Zegenhagen, J. *Nucl. Instrum. Methods Phys. Res.* **1984**, *219*, 430.

(26) Berendsen, H. J. C.; Postma, J. P. M.; van Gunsteren W. F.; Di Nola, A.; Haak, J. R. *J. Chem. Phys.* **1984**, *81*, 3684.

(27) van Gunsteren, W. F.; Berendsen, H. J. C. *Groningen Molecular Simulation (GROMOS) Library Manual*; Biomos: Groningen, 1987.

(28) Åqvist, J.; van Gunsteren W. F.; Leijonmark, M.; Tapia, O. *J. Mol. Biol.* **1985**, *183*, 461.

(29) Straatsma, T. P.; Berendsen, H. J. C.; Postma, J. P. M. *J. Chem. Phys.* **1986**, *85*, 6720.

(30) Berendsen, H. J. C.; Postma, J. P. M.; van Gunsteren W. F.; Hermans, J. In *Intermolecular Forces;* Pullmann, B., Ed.; Reidel: Dordrecht, 1981; p 331.

(31) Ryckaert, J. G., Ciccotti, G.; Berendsen, H. J. C. *J. Comput. Phys.* **1977**, *23*, 327.

(32) Stern, E. A. In *X-ray Absorption: Principles, Applications, Techniques of EXAFS, SEXAFS and XANES*; Koningsberger, D. C., Prins, R., Eds.; John Wiley: New York, 1988; Chapter 1.

(33) Crozier, E. D.; Rehr, J. J.; Ingalls, R. In *X-ray Absorption: Principles, Applications, Techniques of EXAFS, SEXAFS and XANES*; Koningsberger, D. C., Prins, R., Eds.; John Wiley: New York, 1988; Chapter 9, p 373.

(34) Filipponi, A.; Di Cicco, A.; Tyson, T. A.; Natoli, C. R. *Solid. State Commun.* **1991**, *78*, 265. Filipponi, A.; Di Cicco, A. *Synchrotron Radiat. News* **1993**, *6*, 13.

(35) Norman, J. G. *Mol. Phys.* **1976**, *31*, 1191.

(36) Hedin, L.; Lundqvist, B. I. *J. Phys. C* **1971**, *4*, 2064.

(37) Krause, M. O.; Oliver, J. H. *J. Phys. Chem. Ref. Data* **1979**, *8*, 329.

(38) Schaphorst, S. J.; Kodre, A. F.; Ruscheinski, J.; Crasemann, B.; Åberg, T.; Tulkki, J.; Chen, M. H.; Azuma, Y.; Brown, G. S. *Phys. Rev. A* **1993**, *47*, 1953 and references therein. Zhang, K.; Stern, E. A.; Rehr, J. J.; Ellis, F. *Phys. Rev. B* **1991**, *44*, 2030. Filipponi, A.; Tyson, T. A.; Hodgson, K. O.; Mobilio, S. *Phys. Rev. A* **1993**, *48*, 1328. Filipponi, A.; Ottaviano, L.; Tyson, T. A. *Phys. Rev. A* **1993**, *48*, 2098. Chaboy, J.; Marcelli, A.; Tyson, T. A. *Phys. Rev. B* **1994**, *49*, 11652. Di Cicco, A.; Filipponi, A. *Phys. Rev. B* **1994**, *49*, 12564.

(39) D'Angelo, P.; Di Cicco, A.; Filipponi, A; Pavel, N. V. *Phys. Rev. A* **1993**, *47*, 2055.

(40) Burattini, E.; D'Angelo, P.; Di Cicco, A.; Filipponi, A.; Pavel, N. V. *J. Phys. Chem.* **1993**, *97*, 5486.

(41) Filipponi, A.; Ottaviano, L.; Passacantando, M.; Picozzi, P.; Santucci, S. *Phys. Rev. E* **1993**, *48*, 4575.

(42) Bernieri, E.; Balerna, A.; Mobilio, S.; Burattini, E. In *Synchrotron Radiation at Frascati: 1986 Users Meeting; Conference Proceedings of Italian Physical Society*; Mobilio, S., Patella, F.; Stipcich, S., Eds.; Italian Physical Society: Bologna, 1986; Vol. 5, p. 65.

(43) Li, G.; Bridges, F.; Brown, G. S. *Phys. Rev. Lett.* **1992**, *68*, 1609.

(44) Frenkel, A. I.; Stern, E. A.; Qian, M.; Newville, M. *Phys. Rev. B* **1993**, *48*, 12449.

(45) *Handbook of Chemistry and Physics*, 74th ed.; Lide, D. R., Ed.; CRC: Boca Raton, FL, 1993−1994; p 10-266.

(46) Report of the International Workshop on Standards and Criteria in X-Ray Absorption Spectroscopy. *Physica B* **1989**, *158*, 701.

(47) Ludwig, Jr., K. F.; Warburton, W. K.; Fontaine, A. *J. Chem. Phys.* **1987**, *87*, 620.

(48) Bertagnolli, H.; Ertel, T. S.; Hoffmann, M.; Frahm, R. *Ber. Bunsen-Ges. Phys. Chem.* **1991**, *95*, 704.

(49) Bottari, E.; Festa, M. R. *Monatsh. Chem.* **1993**, *124*, 1119.

(50) Bottari, E.; Festa, M. R., unpublished results.

(51) Laurent, T. C.; Persson, H. *Biochim. Biophys. Acta* **1965**, *106*, 616.

(52) Kawamura, H.; Murata, Y.; Yamaguchi, T.; Igimi, H.; Tanaka, M.; Sugihara, G.; Kratohvil, J. P. *J. Phys.Chem.* **1989**, *93*, 3321.

JP941953K